Mechanism and Machine Theory 120 (2018) 192–202

Contents lists available at ScienceDirect

Mechanism and Machine Theory

journal homepage: www.elsevier.com/locate/mechmachtheory

Research paper

Kinematic analysis and multi-objective optimization of a 3-UPR parallel mechanism for a robotic leg

Matteo Russo[a,*], Saioa Herrero[b], Oscar Altuzarra[b], Marco Ceccarelli[a]

[a] LARM, University of Cassino and Southern Latium, Italy
[b] Mechanical Engineering Department, UPV/EHU University of the Basque Country, Spain

ARTICLE INFO

Article history:
Received 29 March 2017
Revised 5 September 2017
Accepted 5 October 2017
Available online 10 October 2017

Keywords:
Parallel manipulator
Multi-objective optimization
Mechanism design
Kinematics
Robotic leg

ABSTRACT

In this paper, a parallel mechanism with 3-UPR architecture for a robotic leg application is analyzed for design purposes. The proposed morphology is characterized by the convergence of the three chains to a single point of the moving platform. First, the mechanism is described and its inverse and forward kinematic problems are solved analytically. Its Jacobian matrix is computed to evaluate the singular positions of the end-effector. Then, workspace volume, manipulator dexterity, static efficiency and stiffness are chosen as objective functions for a multi-objective optimization in order to decide the geometrical parameters of the mechanism. The objective functions are mapped in the parameter space and an optimal solution is discussed as suitable for a future prototype.

1. Introduction

Usually, parallel architectures are not used for robotic legs, since they have a smaller workspace than serial ones of the same size, even if they perform better in terms of accuracy and payload [1–3]. A successful example of a 6-degrees-of-freedom robotic leg with parallel structure is presented in the Waseda locomotor in [4]. Several research teams proposed parallel leg structures with limited mobility. Parallel kinematic manipulators with less than six degrees-of-freedom have several advantages over parallel manipulators with six degrees of freedom in terms of simple structure, easy control and lower cost. Usually, translational 3-degrees-of-freedom parallel mechanisms have a larger workspace than 6-degrees-of-freedom ones.

A lot of effort has been done in the last years in order to find an optimal way to analyse and design this kind of structures [5–7]. The work in [5], for example, deals with the type synthesis of lower-mobility parallel manipulators; Zlatanov, Bonev and Gosselin study constraint singularities in [6], which are typical of this class of mechanisms and which cannot be evaluated by the input-output kinematic relation only. Joshi and Tsai present a way to compute a complete 6×6 Jacobian matrix for lower-mobility manipulators in [7]. Some examples of these structures applied in robotic legs are shown in [8–10]. In particular, Wang et al. [8] describe a reconfigurable biped locomotor based on lower-mobility parallel manipulators. Pan and Gao use 3-DoF legs for an hexapod robot [9], while Wang and Ceccarelli [10] proposed a biped robot with 3-UPU legs that has later been developed in the mechanism optimized in this paper [11–13].

The objective functions for the optimization of lower-mobility parallel mechanisms are discussed in many research works. Carbone et al. [14] proposed an optimization procedure for both serial and parallel robots by using workspace volume,

* Corresponding author.
E-mail addresses: matteo.russo@unicas.it (M. Russo), saioa.herrero@ehu.es (S. Herrero), oscar.altuzarra@ehu.es (O. Altuzarra), ceccarelli@unicas.it (M. Ceccarelli).

https://doi.org/10.1016/j.mechmachtheory.2017.10.004
0094-114X/

Jacobian matrix and compliant displacements. Zhang and Gao [15] optimized their manipulator with a novel performance index, the dexterous design, along with reachable workspace evaluated through forward kinematics. Another 3-DoF mechanism is analysed in [16], where the best algorithms for multi-objective optimization are investigated by using the mean value and the standard deviation of the global distributions as the design indices. The work in [17] presents a framework for multi-criteria design optimization of parallel mechanisms with regards to computational efficiency. A method to identify Pareto-optimal solutions for the design of low-mobility parallel manipulators is presented in [18], while both [19, 20] report the optimization of low-mobility parallel manipulators, a linear Delta parallel robot and a symmetric parallel Schönflies-motion generator, respectively.

This paper analyses a novel 3-DoF parallel manipulator that is based on a 3-UPR architecture. The novel tripod structure was introduced in [11–13]. Section 2 presents a kinematic analysis of the manipulator by solving its inverse and direct kinematic problem and by evaluating its Jacobian matrix. Then, in order to find an optimal design for the mechanism, a multi-objective optimization problem is proposed. Among all the indices that are used to evaluate the workspace of the manipulator, its kinematic and dynamic performance and its stiffness, four indices are chosen and computed in their closed-form expressions in Section 3 for the proposed manipulator, while Section 4 solves the multi-objective optimization by mapping the objective functions in the parameter space and discussing the results in order to find an optimal design.

2. Kinematics of the proposed manipulator

The subject of the paper is the 3 degrees-of-freedom mechanism shown in Fig. 1 and introduced in [11–13]. It is composed by a fixed frame and an end-effector body connected to each other by three UPR chains, characterized by a universal joint U, an actuated prismatic joint P and a revolute joint R. Referring to Fig. 1(a), each chain consists of a linear actuator with length l_i that is connected to the fixed frame by a universal joint in A_i and to the end-effector by a revolute joint, in H. The mechanism is characterized by a particular arrangement of the universal joints on the base. The joints in A_1 and A_2 are oriented in such a way that the rotation takes place around the Y-axis first, then around the X'-axis. However, the joint in A_3 is oriented so that the rotation order is the opposite - around the X-axis first, and then around the Y' -axis. When this happens, the manipulator behaves like a 3-SPR mechanism and can be analysed as such, where S represents a joint with spherical mobility.

Furthermore, the three revolute joints are all located at the end-effector point H thanks to the mechanism shown in Fig. 1(d) and (e): one of the three connected links, labelled link 1 in Fig. 1(d), rotates around the U-axis of the end-effector mechanism, while link 2 and link 3 of Fig. 1(d) can only rotate around the V-axis. This particular configuration of the end-effector simplifies the kinematics of the structure, since the position of point H can be found as the intersection of three spheres centred at A_i with radius equal to l_i, for $i = \{1, 2, 3\}$. Therefore, if the base frame is an equilateral triangle with side length a to give

$$ {}^0\boldsymbol{A}_1 = \begin{pmatrix} 0 \\ 0 \\ 0 \end{pmatrix};\ {}^0\boldsymbol{A}_2 = \begin{pmatrix} a \\ 0 \\ 0 \end{pmatrix};\ {}^0\boldsymbol{A}_3 = \begin{pmatrix} a/2 \\ \sqrt{3}\ a/2 \\ 0 \end{pmatrix} \tag{1} $$

The inverse kinematic problem of the structure can be solved as

$$ \begin{aligned} l_1 &= \sqrt{x^2 + y^2 + z^2} \\ l_2 &= \sqrt{(x-a)^2 + y^2 + z^2} \\ l_3 &= \sqrt{(x-b)^2 + (y-c)^2 + z^2} \end{aligned} \tag{2} $$

where x, y, z are the absolute coordinates of the end point H.

From Eq. (2) the direct kinematic problem can be expressed as

$$ \begin{aligned} x &= \frac{1}{2a}\left({l_1}^2 - {l_2}^2 + a^2\right) \\ y &= \frac{1}{2\sqrt{3}a}\left({l_1}^2 + {l_2}^2 - 2{l_3}^2 + a^2\right) \\ z &= -\sqrt{\frac{-{l_1}^4 - {l_2}^4 - {l_3}^4 - a^4 + {l_1}^2{l_2}^2 + {l_1}^2{l_3}^2 + {l_2}^2{l_3}^2 + a^2\left({l_1}^2 + {l_2}^2 + {l_3}^2\right)}{3a^2}} \end{aligned} \tag{3} $$

Non-equilateral configuration for the base frame have been investigated but held worse results than the reported ones for the equilateral triangle. This paper analyses and gives the optimization of this particular configuration only.

The Jacobian of the structure can be obtained from differentiation of Eqs. (2) and (3). The result is a 3×3 matrix given by

$$ \boldsymbol{J_p} = \begin{bmatrix} \frac{l_1}{a} & -\frac{l_2}{a} & 0 \\ \frac{l_1}{\sqrt{3}a} & \frac{l_2}{\sqrt{3}a} & -\frac{2l_3}{\sqrt{3}a} \\ \frac{l_1}{z}\left(1 - \frac{x}{a}\right) - \frac{yl_1}{\sqrt{3}az} & \frac{l_2}{az}\left(x - \frac{y}{\sqrt{3}}\right) & \frac{2yl_3}{\sqrt{3}az} \end{bmatrix} \tag{4} $$

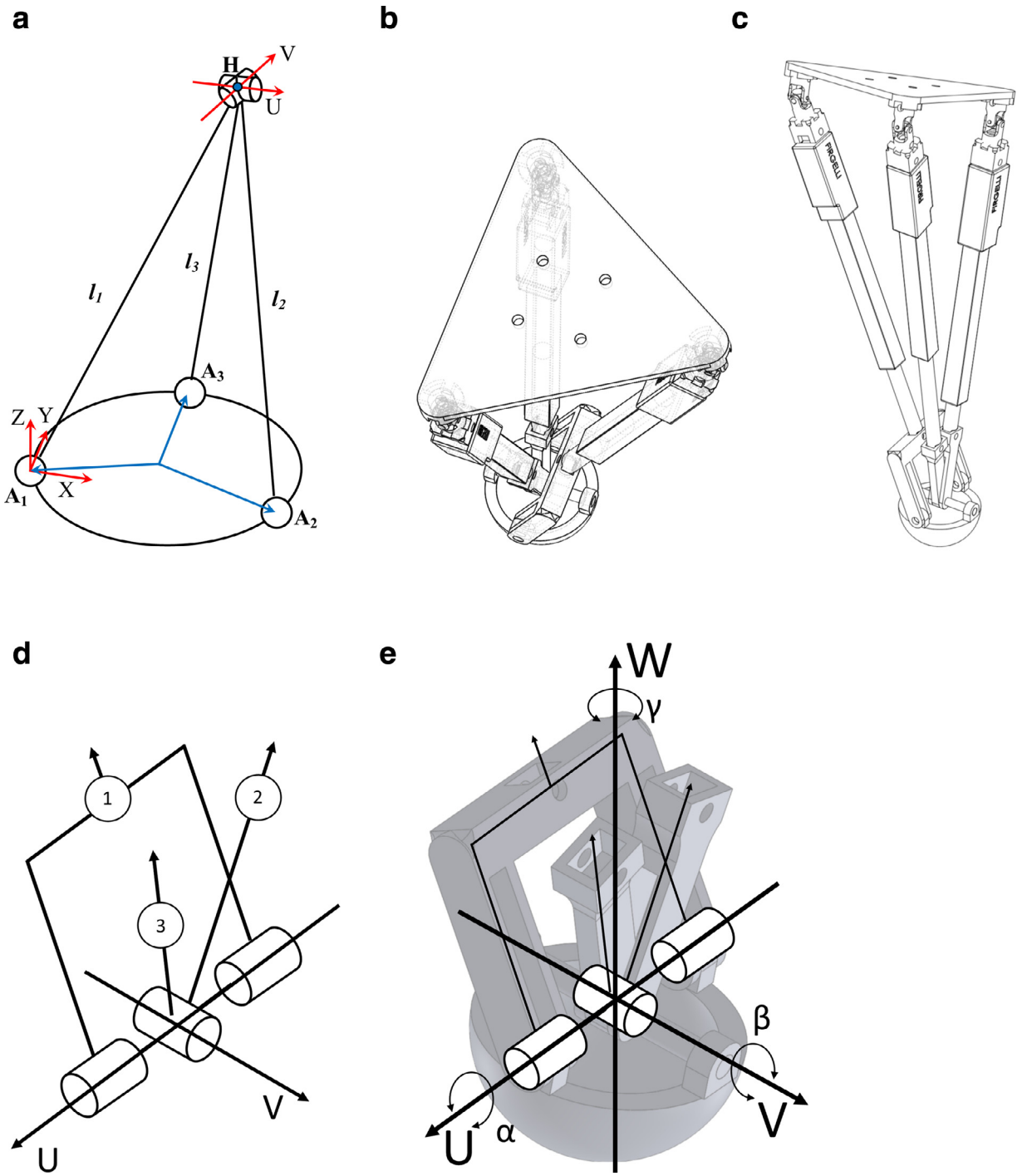

Fig. 1. The proposed mechanism: (a). kinematic diagram of the tripod structure; (b). CAD design of the manipulator, upper view; (c). CAD design of the manipulator, side view; (d). kinematic diagram of the end-effector mechanism; (e). CAD design of the end-effector mechanism.

The inverse Jacobian can be computed from Eq. (4) as

$$\boldsymbol{J_p}^{-1} = \begin{bmatrix} \frac{x}{l_1} & \frac{y}{l_1} & \frac{z}{l_1} \\ \frac{x-a}{l_2} & \frac{y}{l_2} & \frac{z}{l_2} \\ \frac{x-\frac{a}{2}}{l_3} & \frac{y-\frac{\sqrt{3}a}{2}}{l_3} & \frac{z}{l_3} \end{bmatrix} \tag{5}$$

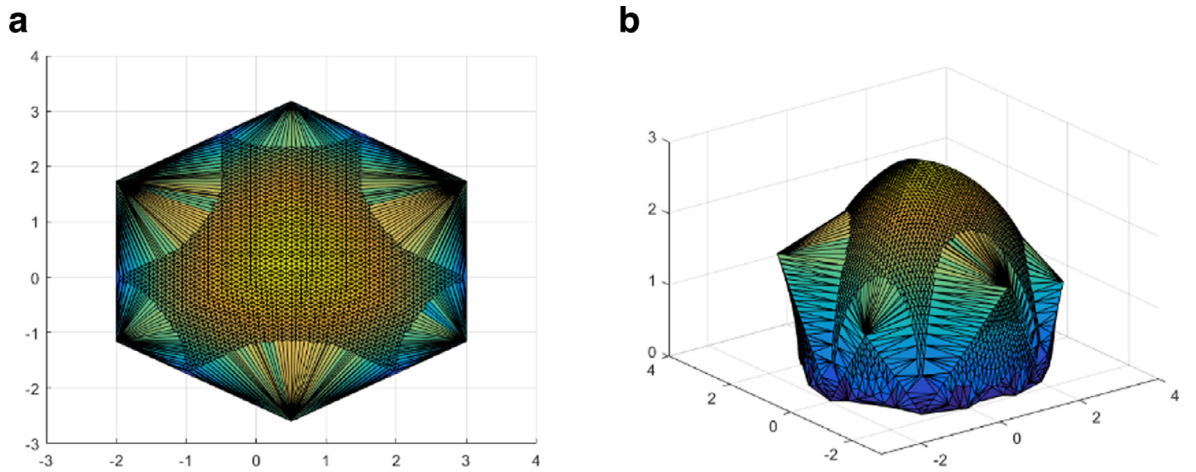

Fig. 2. Computed reachable workspace of the mechanism for a = 1, lmin = 2a, lmax = 3a; a. upper view; b. isometric view.

The singularities of the mechanism can be evaluated by using Eq. (4). The Jacobian matrix is singular only in the plane $z = 0$, where the end-effector cannot physically go due to the limitations of the joints. Therefore, the reachable workspace of the mechanism can be obtained by computing

$$\boldsymbol{H} = (x,\ y, z)^T \ for\ l_1,\ l_2,\ l_3 \in [l_0, l_0 + s] \tag{6}$$

and it is coincident with its singularity-free workspace.

The kinematic problem of the manipulator is written in position only and not in orientation because the end-effector is analytically described as a punctiform body. However, it is possible to evaluate the orientation of the UVW coordinate system at the revolute pairs at H from constraint equations as

$$\begin{aligned} \alpha &= \tan^{-1} \frac{\left(l_1{}^2+l_2{}^2-2l_3{}^2+a^2\right)}{2\sqrt{-l_1{}^4-l_2{}^4-l_3{}^4-a^4+l_1{}^2l_2{}^2+l_1{}^2l_3{}^2+l_2{}^2l_3{}^2+a^2\left(l_1{}^2+l_2{}^2+l_3{}^2\right)}} \\ \beta &= \tan^{-1} \frac{l_1{}^2-l_2{}^2}{\sqrt{4a^2l_3{}^2-l_2{}^4-l_1{}^4+2l_1{}^2l_2{}^2}} \\ \gamma &= 0 \end{aligned} \tag{7}$$

where α is the intrinsic rotation angle of the end effector around the X-axis, β is the intrinsic rotation around the Y'-axis, and γ is the intrinsic rotation around the Z"-axis.

3. Kinematic and dynamic performance

In order to optimise the geometry of the mechanism, its kinematic and dynamic performance has to be evaluated. The four different functions proposed in the next sub-sections have been devised as numerical indices to compute both the kinematic and dynamic performance of the parallel mechanism.

3.1. Workspace volume

The workspace volume is a criterion that can be used as objective function for optimization [2]. The maximal or reachable workspace, which includes all the points that can be reached by the end-effector with at least one orientation, is significant for the proposed structure, since orientation and position are dependant. Therefore, one criterion for the optimisation can be the reachable workspace volume, which is expressed as

$$V = \begin{cases} H = (x(l_1,\ l_2,\ l_3),\ y(l_1,\ l_2,\ l_3), z(l_1,\ l_2,\ l_3))^T \\ \qquad for\ l_1,\ l_2,\ l_3 \in [l_0, l_0 + s] \end{cases} \tag{8}$$

Fig. 2 shows the reachable workspace of the proposed mechanism for $a = 1$, $l_{min} = 2a$, $l_{max} = 3a$.

As seen in Fig. 2, the shape of the reachable workspace of the mechanism is irregular and its implementation in control algorithm for particular trajectories can be difficult. Therefore, a workspace with a simpler shape is preferred. Since the proposed mechanism has axial symmetry, it is possible to define its operational workspace as all the circular trajectory on the XY plane that can be reached by the end-effector. Thus, the operational workspace is expressed as

$$V_o = \begin{cases} c_k(z) = \left\{(x(z),\ y(z)) \in \mathbb{R}^2 : x^2(z) + y^2(z) = r_i{}^2(z)\right\}\ for \\ \qquad \boldsymbol{q}^T \in \mathbb{R}^n,\ \forall\ i = 0,\ \ldots,\ m,\ \forall k = 0,\ \ldots,\ l \end{cases} \tag{9}$$

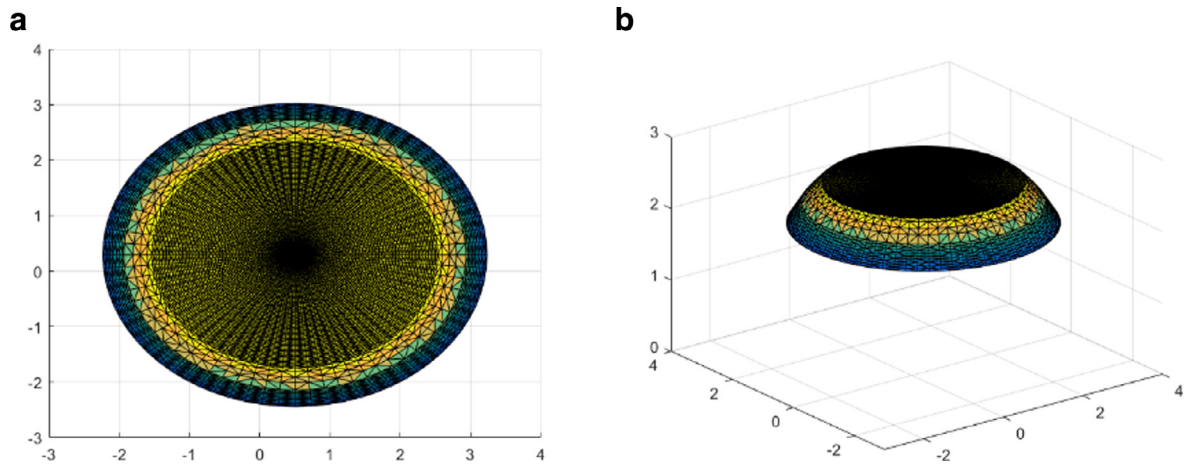

Fig. 3. Computed workspace as maximum circular trajectories of the mechanism for a = 1, lmin = 2a, lmax = 3a; a. upper view; b. isometric view.

where V_o is the volume of the workspace, r_i is the radius of the circular trajectory $c_k(z)$ in each *xy* plane up to the maximum radius r_m, which is the radius of the last discrete point that verifies the inverse position problem, and l is the maximum number of trajectories in V_o. Fig. 3 illustrates an example of operational workspace for the same design that is used for the generation of the workspace in Fig. 2.

3.2. Dexterity

The dexterity of a robot refers to an error on the end-effector position as the result of a position error in the actuation [1,19]. A robot with high dexterity has a low amplification factor between the input error and output displacement. A leg mechanism should have high dexterity for dynamic walking, since errors in the positioning of the foot could result in loss of balance. The Jacobian matrix allows to establish a linear relation between the manipulator accuracy $\delta_{\boldsymbol{x}} = (\delta_x, \delta_y, \delta_z)$ and the measurement error $\delta\boldsymbol{q}$ on $\boldsymbol{q} = (l_1, l_2, l_3)$. The error hyper-sphere in the joint space is defined as

$$\|\delta\boldsymbol{q}\| \leq 1 \tag{10}$$

and can be mapped into an ellipsoid in the generalized Cartesian error space, which is called manipulability ellipsoid and can be written as

$$\|\delta\boldsymbol{q}\| \leq 1 \Rightarrow \delta\boldsymbol{x}^T \boldsymbol{J_p}^{-T} \boldsymbol{J_p}^{-1} \delta\boldsymbol{x} \leq 1 \tag{11}$$

The shape and volume of this ellipsoid characterize the manipulator dexterity. When one of the axis of this ellipsoid is large, there is a large amplification factor between the errors in the actuated joint measurements errors and the positioning error of the end-effector for a given combination of sensor errors. Several indices can be extracted from Eq. (11) in order to quantify the dexterity of a mechanism, when it refers to the capability of the end-effector to move in an arbitrary direction. The most commonly used indices are Yoshikawa's manipulability index and the condition number [1,14,17,19]. The manipulability index for the mechanism under examination is defined as

$$w = \sqrt{\left\|\boldsymbol{J_p}\boldsymbol{J_p}^T\right\|} = \frac{2l_1 l_2 l_3}{\sqrt{3}a^2 z} \tag{12}$$

The condition number is a direct measure of the amplification of the position error in the actuators onto the end-effector position in a given configuration, as given by Eq. (11) [1]. It is expressed as

$$\kappa = \|\boldsymbol{J_p}\| \left\|\boldsymbol{J_p}^{-1}\right\| \tag{13}$$

The norm of the Jacobian in Eq. (13) can be expressed in several ways, such as the Euclidean norm, the infinite norm and the Frobenius norm. However, the Frobenius norm is preferred for parallel manipulators [12]. Thus, the norm of the Jacobian of the proposed structure can be computed as

$$\|\boldsymbol{J_p}\| = \sqrt{\sum_{i=1}^{3}\sum_{j=1}^{3} abs\left(a_{ij}\right)^2} = \sqrt{\frac{1}{3} tr\left(\boldsymbol{J_p}\boldsymbol{J_p}^T\right)} \tag{14}$$

Therefore, the global conditioning index for the mechanism under examination is equal to

$$\begin{aligned}\kappa &= \boldsymbol{J_p}\boldsymbol{J_p}^{-1} = \tfrac{1}{3}\sqrt{\sum_{i=1}^{3}\left(12\left|\tfrac{l_i}{a}\right|^2 + \left|\tfrac{l_i k_i}{a^2 z}\right|^2\right)}\\ k_1 &= -2{l_1}^2 + {l_2}^2 + {l_3}^2 + a^2\\ k_2 &= {l_1}^2 - 2{l_2}^2 + {l_3}^2 + a^2\\ k_3 &= {l_1}^2 + {l_2}^2 - 2{l_3}^2 + a^2\end{aligned} \tag{15}$$

The condition number evaluates the dexterity of the manipulator in a single point of its workspace. A single value able to represent the dexterity of the manipulator in its entire workspace is needed to define a proper objective function. A global conditioning index can be proposed as Eq. (16) to be used as an optimization criterion.

$$\epsilon_g = \frac{1}{V}\iiint_V \frac{1}{\kappa} dV \tag{16}$$

3.3. Force transmission

In order to evaluate the static performance of the manipulator, it is necessary to write the vector of actuation forces and the wrench respectively as

$$\boldsymbol{\tau} = \begin{pmatrix}\tau_1\\ \tau_2\\ \tau_3\end{pmatrix};\ \boldsymbol{f} = \begin{pmatrix}f_1\\ f_2\\ f_3\end{pmatrix} \tag{17}$$

By applying the principle of virtual work, the relation between input actuation forces and the output wrench is expressed as

$$\boldsymbol{f}^T\dot{\boldsymbol{x}} - \boldsymbol{\tau}^T\dot{\boldsymbol{q}} = 0 \tag{18}$$

Since for a given motion the velocity of the end-effector is different from 0, it is possible to write Eq. (18) as

$$\boldsymbol{f} = \boldsymbol{J_p}^{-T}\boldsymbol{\tau} \tag{19}$$

and by defining a wrench that is bonded by

$$\|\boldsymbol{f}\| \leq 1 \tag{20}$$

It is possible to evaluate the maximal joint forces for a given pose and load of the manipulator. This representation is similar to the one used for the velocity ellipsoid, and the force ellipsoid can be described as

$$\boldsymbol{\tau}^T\boldsymbol{J_p}^{-1}\boldsymbol{J_p}^{-T}\boldsymbol{\tau} \leq 1 \tag{21}$$

Thus, it is possible to define a local force manipulability index for the proposed mechanism as

$$w_f = \sqrt{\left\|\boldsymbol{J_p}^{-T}\boldsymbol{J_p}^{-1}\right\|} = \frac{\sqrt{3}a^2 z}{2l_1 l_2 l_3} \tag{22}$$

and a global force transmission index can be deduced from Eq. (22), given by

$$\epsilon_f = \frac{1}{V}\iiint_V w dV \tag{23}$$

However, this index does not take into account the application of the mechanism as a robotic leg. The following index is introduced to evaluate the efficiency of the leg as

$$\eta = \frac{\|\boldsymbol{f}\|}{\sum_{i=1}^{3}\|\tau_i\|} \tag{24}$$

When the foot of the robot is in contact with the ground and in quasi-static conditions, the reaction of the ground can be assumed as vertical, while its magnitude depends on the weight of the robot. Therefore, the wrench can be defined as

$$\boldsymbol{f_s} = \begin{pmatrix}0\\ 0\\ r_{ground}\end{pmatrix} \tag{25}$$

where the only non-zero component is the reaction force between end-effector and ground, which is along the z-axis. The efficiency index in Eq. (24) compares this wrench applied to the end effector to the actuations in the linear motors needed to balance it. The index is position dependent, since the reaction can be balanced only by the Z-component of the motor forces, which have the same orientation as each limb, and the ratio between wrench and actuation forces becomes smaller

for positions that are closer to the border of the workspace. Thus, the index in Eq. (24) is a measure of the mechanical advantage of the system for a given position. For the proposed leg mechanism, it is possible to write Eq. (24) as

$$\eta = \frac{\left|a^2 z\right|}{\sum_{i=1}^{3} |l_i k_i|} \tag{26}$$

There is no dependency on the magnitude of the wrench, since only the geometry of the system appears in Eq. (26). Therefore, the index is a suitable optimization criterion to be used as objective function.

3.4. Stiffness

Stiffness plays a key role in the control of any robotic system, and it is important to include it as design criterion. In particular, the joint stiffness should be modelled in order to get a performing control system. The stiffness of the mechanism under study can be evaluated by using an elastic model for the variation of the joint variables, as

$$\Delta \boldsymbol{\tau} = k \Delta \boldsymbol{q} \tag{27}$$

where k is the elastic stiffness of the link, which is supposed to be identical for the three actuators. Thus, when

$$\Delta \boldsymbol{q} = \boldsymbol{J_p}^{-1} \Delta \boldsymbol{x};\ \Delta \boldsymbol{f} = \boldsymbol{J_p}^{-T} \Delta \boldsymbol{\tau} \tag{28}$$

it is possible to write Eq. (28) as

$$\Delta \boldsymbol{f} = \boldsymbol{J_p}^{-T} k \boldsymbol{J_p}^{-1} \Delta \boldsymbol{x} \tag{29}$$

Thus, the stiffness matrix $\mathbf{K}$ is defined as

$$\boldsymbol{K} = k \boldsymbol{J_p}^{-T} \boldsymbol{J_p}^{-1} \tag{30}$$

The norm of the stiffness matrix of the robot in a certain configuration, when $k = 1$, it can be expressed as

$$K = \left|\boldsymbol{J_p}^{-T} \boldsymbol{J_p}^{-1}\right| = \left(\frac{\sqrt{3} a^2 z}{2 l_1 l_2 l_3}\right)^2, \tag{31}$$

and can be chosen as objective function to represent the stiffness of the manipulator.

4. Multi-objective optimization and results

A multi-objective optimization is the research of an optimal set of parameters, which are subject to constraint functions, with regards to two or more objective functions [14]. The problem can be defined as

$$\begin{aligned} &\min \boldsymbol{F}(\boldsymbol{r}) = \min [f_1(\boldsymbol{r})\ f_2(\boldsymbol{r}) \cdots f_n(\boldsymbol{r})]^T, \qquad \boldsymbol{r} = [r_1\ r_2 \cdots\ r_m]^T \\ &\textit{with } \boldsymbol{F} : \mathbb{R}^m \to \mathbb{R}^n,\ \boldsymbol{F}(\boldsymbol{r}) = [f_1(\boldsymbol{r})\ f_2(\boldsymbol{r}) \cdots f_n(\boldsymbol{r})]^T \\ &\textit{subject to } \boldsymbol{g}(\boldsymbol{r}) \le 0,\ \boldsymbol{h}(\boldsymbol{r}) = 0 \\ &\textit{with } \boldsymbol{g}(\boldsymbol{r}) = [g_1(\boldsymbol{r})\ g_2(\boldsymbol{r}) \cdots g_p(\boldsymbol{r})]^T \\ &\textit{and } \boldsymbol{h}(\boldsymbol{r}) = [h_1(\boldsymbol{r})\ h_2(\boldsymbol{r}) \cdots h_t(\boldsymbol{r})]^T \end{aligned} \tag{32}$$

where $\boldsymbol{F}$ is the vector that contains the objective functions f_i, $\boldsymbol{r}$ is the vector of the design parameters of the system, $\boldsymbol{g}$ is the disequality constraint function vector and $\boldsymbol{h}$ the equality constraint function vector. The numbers n, m, p and t describe respectively the number of objective functions, design parameters, disequality constraints and equality constraints.

The problem is solved by finding the optimal set of design parameters [19–20], which are called *Pareto-optimal* or *non-dominated* and are those solutions which cannot be improved in any of the objectives without degrading at least another one. The objective functions chosen for the analysis are four: workspace volume, global conditioning index, force efficiency and stiffness parameters, shown respectively as Eqs. (9), (16), (26) and (31).

The multi-optimization problem only needs two parameters in order to fully define the geometry of the proposed manipulator. These parameters are the ratio of the stroke of the actuator s over the base dimension a and the ratio of the minimum length of each leg l_0 over the base dimension a. Thus, vector $\boldsymbol{r}$ is equal to $(s/a,\ l_0/a)$ and it is possible to employ an exhaustive method that directly generates all the solutions by computing the value of each objective function for each possible combination of the design parameters within the chosen range.

The constraint functions for the attached problem can be written as

$$\frac{l_{0,min}}{a} \le \frac{l_0}{a} \le \frac{l_{0,max}}{a};\ \frac{s_{min}}{a} \le \frac{s}{a} < \frac{l_0}{a} \tag{33}$$

where the maximum length of the stroke is limited by the minimum length of the actuator for physical limitations. Given Eq. (33) with the numerical constraints defined by

$$0.9 \le \frac{l_0}{a} \le 2;\ 0.9 \le \frac{s}{a} < \frac{l_0}{a} \tag{34}$$

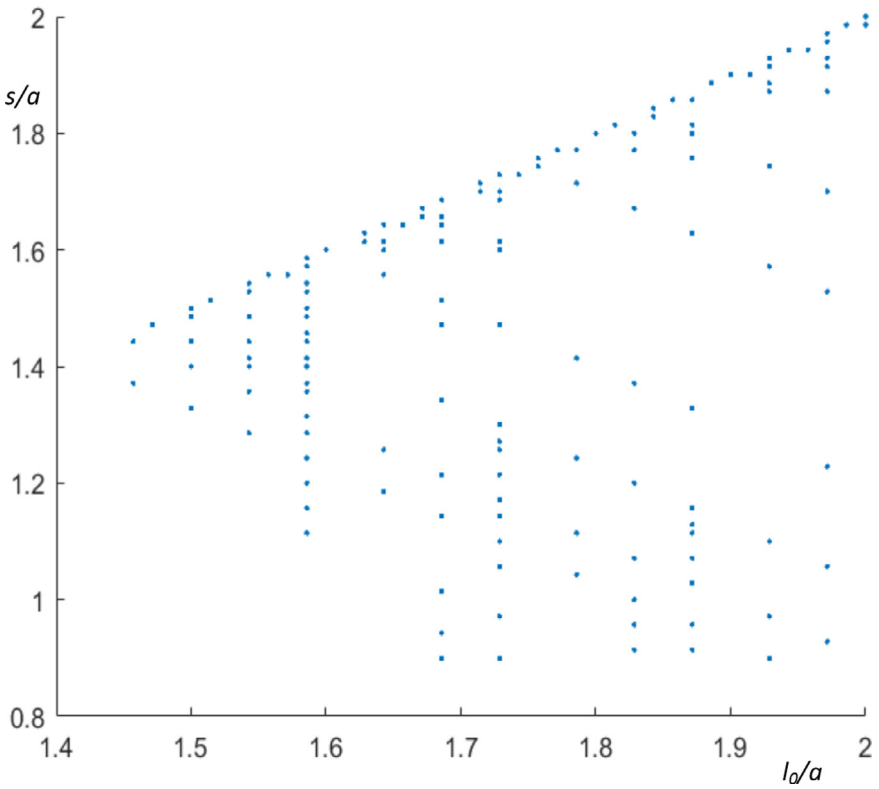

Fig. 4. Points of the parameter space belonging to the Pareto front of the multi-objective optimization problem in Eq. (32).

It is possible to compute the Pareto front for the problem. The results are the points in Fig. 4. The optimal values are scattered in the whole parameter space and do not give relevant information about the values of the objective functions in each point. Therefore, it is difficult to define a single optimal solution by analysing only the Pareto front. In order to get an optimal set of parameters, the following procedure has been followed:

- Evaluation of the objective functions: each objective function is computed in the parameter space;
- Computation of displacements: a mean value of each objective function in the parameter space is computed. Then, in each point of the parameter space, the displacement from the mean value has been obtained for each objective function;
- Performance map: a performance map is plotted with the data obtained in the previous points by assigning to each region of the parameter space the number of objective functions with displacement over a threshold value. The optimal threshold value is defined as the value for which no more than 5% of the parameter space contains all the objective function over the threshold value itself;
- Optimal solutions: the optimal parameter sets are the regions of the parameter space where all the objective functions are over the threshold value.

Thus, each objective function has been plotted in the parameter space in order to get additional information towards an optimal solution. Figs. 5-8 illustrate how the objective functions vary with regards to different configurations by mapping their displacement from the mean value, which can be computed as

$$\Delta f_i\left(\frac{l_0}{a},\ \frac{s}{a}\right) = \frac{f_i\left(\frac{l_0}{a},\ \frac{s}{a}\right)}{f_{i,mean}} \tag{35}$$

As shown in Figs. 5-8, some objective functions are influenced more than others by the two optimization parameters. In particular, the efficiency function presented in Eq. (26) is characterized by a maximum variation of 20% from its average value (Fig. 6), while for the dexterity, in Fig. 5, the maximum variation is over 50%. Both workspace volume and stiffness vary over 100% of their average value in the parameter space, as shown in Figs. 5 and 8. Furthermore, the optimum of each objective function is located in a different region of the parameter space. While both stiffness and dexterity are at their maximum for minimum l_0 and minimum s, a good efficiency can be found for small values of the stroke. However, it does not show a dependency on the minimum length of the link. Finally, the workspace volume is optimized in a different region, characterized by high values of both the optimization parameters. Therefore, it is impossible to get an optimum value and optimal solutions should be studied in order to find a compromise between the different objectives.

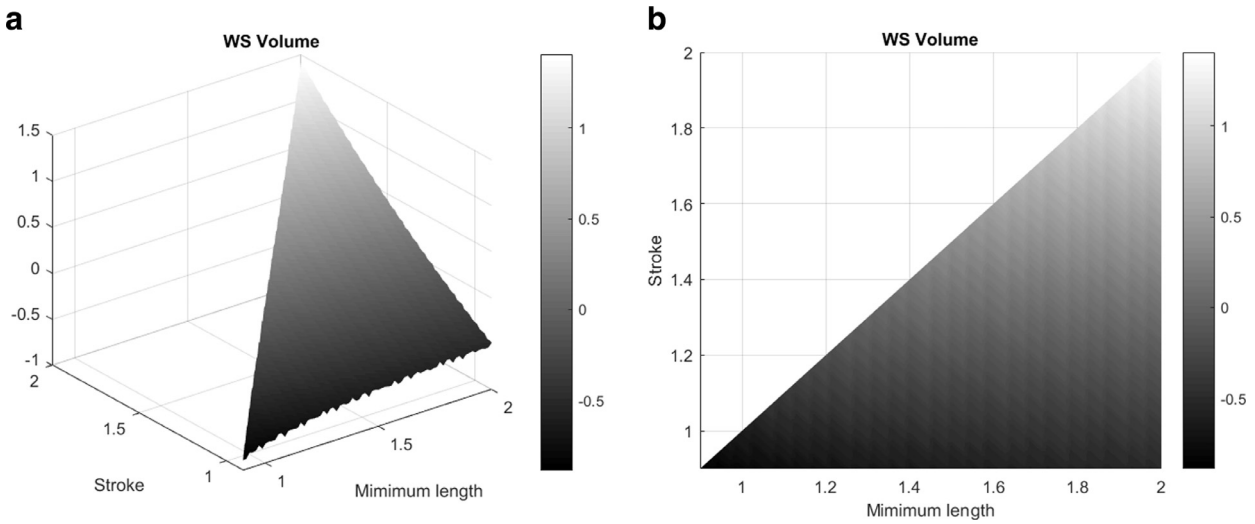

Fig. 5. Workspace volume objective function of Eq. (9) plotted in the parameter space: a. 3D representation; b. 2D map.

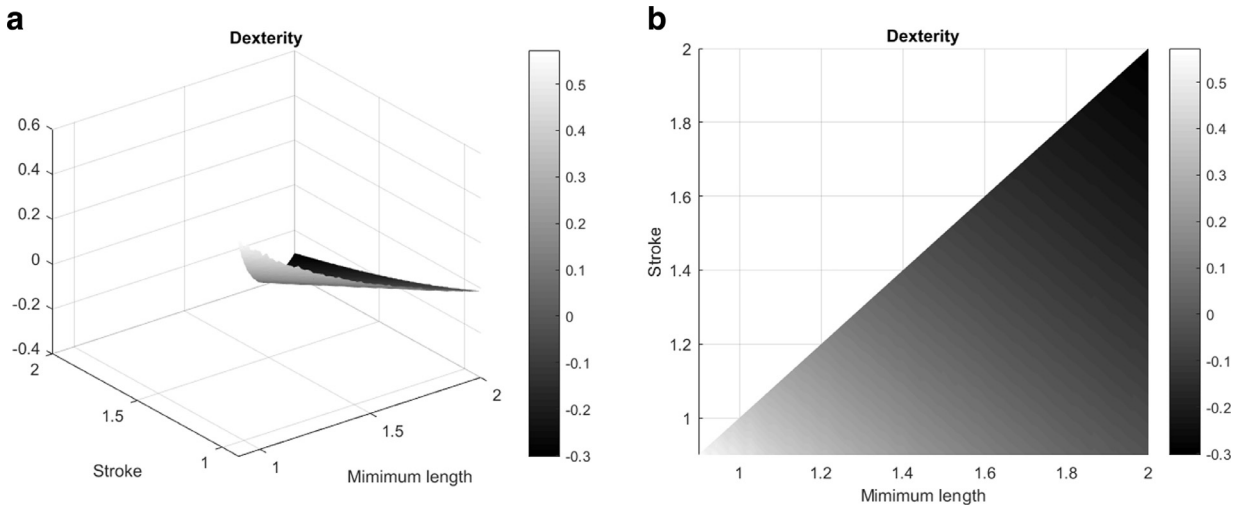

Fig. 6. Dexterity objective function of Eq. (16) plotted in the parameter space: a. 3D representation; b. 2D map.

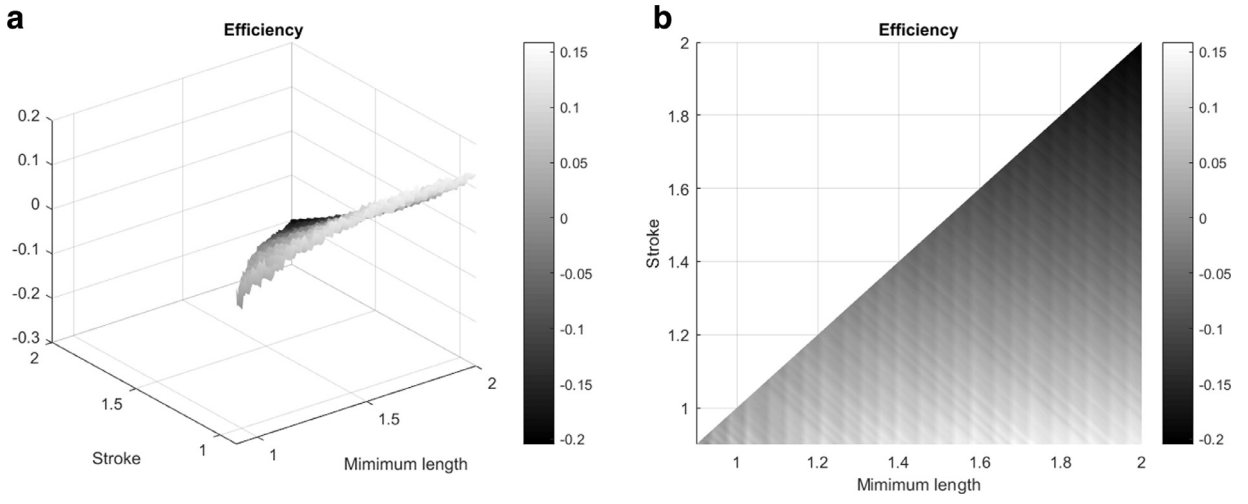

Fig. 7. Force efficiency objective function of Eq. (26) plotted in the parameter space: a. 3D representation; b. 2D map.

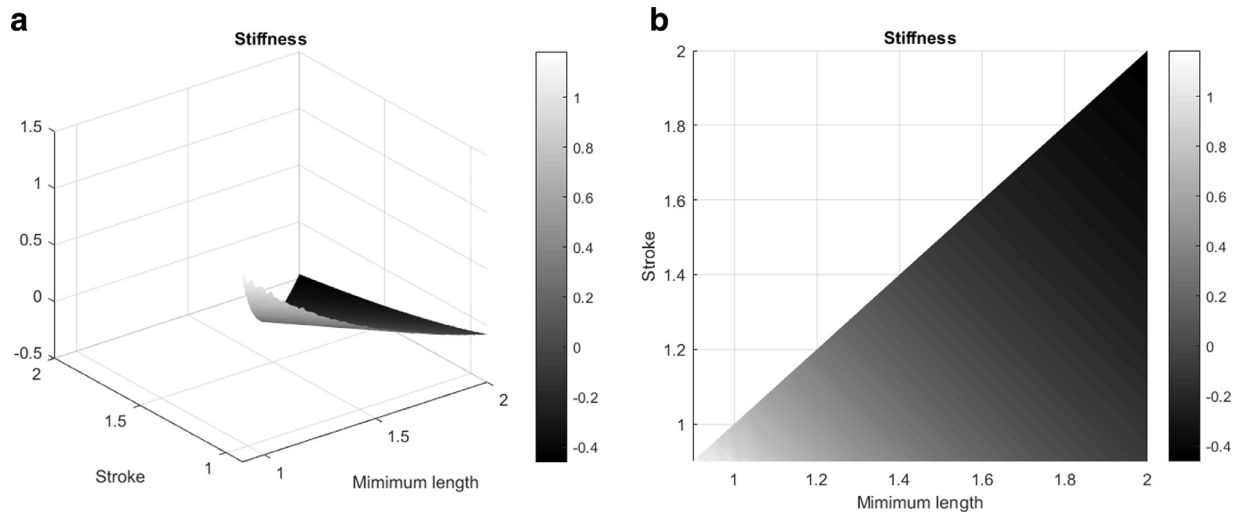

Fig. 8. Stiffness objective function of Eq. (31) plotted in the parameter space: a. 3D representation; b. 2D map.

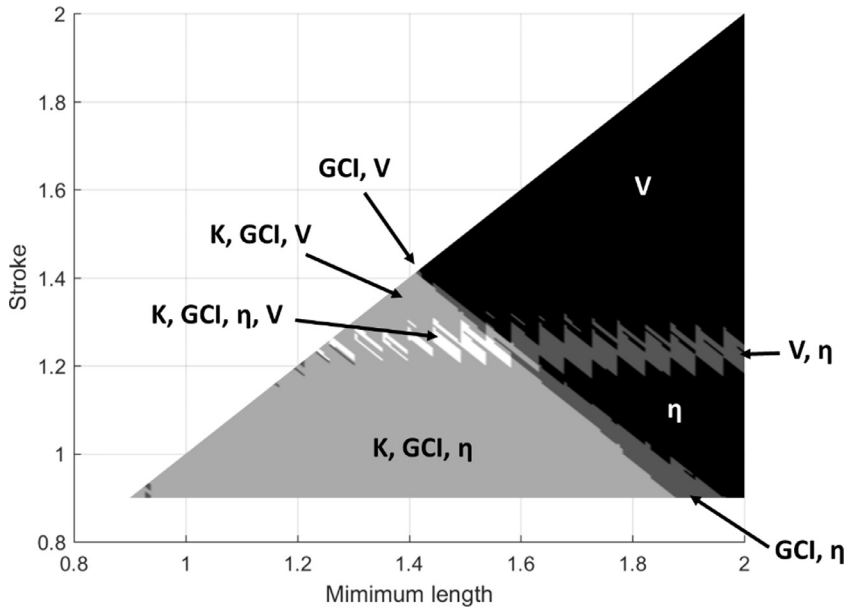

Fig. 9. Objective functions with positive displacement from the mean value in different regions of the parameter space. V: workspace volume; GCI: dexterity; η: force efficiency; K: stiffness.

The performance map in Fig. 9 divides the parameter space in eight regions. In each region, the value of the displacement from the mean value of a certain number of objective function is greater than the threshold, set to 0. The parameter sets in the inner white region of Fig. 9 are assumed to be the optimal design solution, since all the objective functions are above average. Therefore, the best design results are obtained around parameter set (1.50, 1.20).

However, some applications could require a smaller workspace but higher dexterity, stiffness and efficiency or *vice versa*. In those cases, the optimization problem can be solved by removing the non-relevant objective function and finding an optimal value for the remaining ones. For example, when the workspace volume is not considered the optimal solution is close to the point (1, 0.9), while the maximum volume is obtained for (2, 2).

5. Conclusions

This paper presents the kinematic analysis and optimization for a 3-DoFs robot leg with 3-UPR architecture. This parallel manipulator is characterized by the specific design of the end-effector, where all its three limbs converge into a single point. Both the forward and inverse kinematic problems are solved and the Jacobian matrix of the manipulator is computed. Con-

sidering joint limitations, the structure is characterized by the absence of singular point in its workspace. Another advantage of the novel structure proposed in the paper is the closed-form expression for both kinematics and Jacobian matrix, which leads to a robust control and a better evaluation of the performance of the mechanism.

A multi-objective optimization has been performed to get optimal geometrical proportions for the links of the mechanism. Four different objective functions are taken into account: workspace volume, dexterity (evaluated with the global conditioning index), mechanical advantage and stiffness. These functions are evaluated through an exhaustive method and the results of the optimization process are discussed in order to define the optimal solution. Since the results obtained with the computation of the Pareto front are not convenient for the definition of an optimal set of parameters, an alternative procedure that considers the behaviour of the objective functions in the workspace has been proposed. Thus, the optimal solution has been found in the set $s/a = 1.20$ and $l_0/a = 1.50$.

Acknowledgements

The first author gratefully acknowledges the period of research he spent within Erasmus + program in 2016 at the UPV/EHU University of the Basque Country under the supervision of Prof. O. Altuzarra.

References

[1] J.P. Merlet, Parallel Robots, 74, Springer, Dordrecht, 2012.
[2] M. Ceccarelli, Fundamentals of Mechanics of Robotic Manipulation, 27, Springer, Dordrecht, 2004.
[3] L.W. Tsai, Robot Analysis: The Mechanics of Serial and Parallel Manipulators, John Wiley & Sons, New York, NY, 1999.
[4] H.O. Lim, A. Takanishi, Biped walking robots created at Waseda University: WL and WABIAN family, Philos. Trans. R. Soc. Lond. A 365 (1850) (2007) 49–64.
[5] Z. Huang, Q.C. Li, General methodology for type synthesis of symmetrical lower-mobility parallel manipulators and several novel manipulators, Int. J. Robot. Res. 21 (2) (2002) 131–145.
[6] D. Zlatanov, I.A. Bonev, C.M. Gosselin, Constraint singularities of parallel mechanisms, in: IEEE International Conference on Robotics and Automation (ICRA 2002), 1, Washington, D.C., 2002, pp. 496–502. 11–15.
[7] S.A. Joshi, L.W. Tsai, "Jacobian Analysis of limited-DOF parallel manipulators, ASME J. Mech. Des. 124 (2002) 254–258.
[8] H. Wang, L. Sang, X. Zhang, X. Kong, Y. Liang, D. Zhang, Redundant actuation research of the quadruped walking chair with parallel leg mechanism, in: IEEE International Conference on Robotics and Biomimetics (ROBIO), IEEE, 2012, pp. 223–228.
[9] Y. Pan, F. Gao, A new six-parallel-legged walking robot for drilling holes on the fuselage, in: Proceedings of the Institution of Mechanical Engineers, Part C: Journal of Mechanical Engineering Science, 228, 2014, pp. 753–764.
[10] M. Wang, M. Ceccarelli, Design and simulation of walking operation of a cassino biped locomotor, in: New Trends in Mechanism and Machine Science, Springer International Publishing, 2015, pp. 613–621.
[11] M. Russo, M. Ceccarelli, Kinematic design of a tripod parallel mechanism for robotic legs, in: Mechanisms, Transmissions and Applications, Springer International Publishing, 2018, pp. 121–130.
[12] Ceccarelli, M., Russo, M., (2016). "Device for the spherical connection of three bodies", IT Patent Application n° 102016000009369 (in Italian 19/09/ 2016).
[13] Russo, M., Cafolla, D., Ceccarelli, M., (2016). "Device for tripod leg", IT Patent Application n° 102016000097258 (in Italian 28/09/ 2016).
[14] G. Carbone, E. Ottaviano, M. Ceccarelli, An optimum design procedure for both serial and parallel manipulators, in: Proceedings of the Institution of Mechanical Engineers, Part C: Journal of Mechanical Engineering Science, 221, 2007, pp. 829–843.
[15] D. Zhang, Z. Gao, Forward kinematics, performance analysis, and multi-objective optimization of a bio-inspired parallel manipulator, Robot. Comput.-Integr. Manuf. 28 (4) (2012) 484–492.
[16] Z. Gao, D. Zhang, X. Hu, Y. Ge, Design, analysis, and stiffness optimization of a three degree of freedom parallel manipulator, Robotica 28 (03) (2010) 349–357.
[17] R. Unal, G. Kiziltas, V. Patoglu, Multi-criteria design optimization of parallel robots, in: 2008 IEEE Conference on Robotics, Automation and Mechatronics, IEEE, 2008, pp. 112–118.
[18] O. Altuzarra, C. Pinto, B. Sandru, A. Hernandez, Optimal dimensioning for parallel manipulators: workspace, dexterity, and energy, J. Mech. Des. 133 (4) (2011) 041007.
[19] R. Kelaiaia, O. Company, A. Zaatri, Multiobjective optimization of a linear Delta parallel robot, Mech. Mach. Theory 50 (2012) 159–178.
[20] O. Altuzarra, A. Hernandez, O. Salgado, J. Angeles, Multiobjective optimum design of a symmetric parallel Schönflies-motion generator, J. Mech. Des. 131 (3) (2009) 031002.